Original Article

Isolated and Grid-Connected Hybrid Microgrid Model Frequency Stabilization by Novel Salp-Swarm Optimization Algorithm

V. Devaraj[1], M. Kumaresan[2]

[1]*Department of Electrical and Electronics Engineering, Dr. M.G.R. Educational and Research Institute, Chennai, Tamil Nadu, India*
[2]*Department of Electronics and Communication Engineering, Dr. M.G.R. Educational and Research Institute, Chennai, Tamil Nadu, India*

[1]*Corresponding Author : djran14@gmail.com*

Abstract - In the case of hybrid power generation systems, frequency deviation is a serious concern. Load frequency control of a Fuel cell, solar and wind-based hybrid power generation system is interconnected with a microgrid. Proportional-Integral-Derivative (PID), Fuzzy Tuned - PID (FT-PID), and PID controllers are utilized (one at a time) to manage the governor of the SPG and pitch of the WTG to improve frequency stabilization of the system. Moreover, Salp-Swarm Optimization Algorithm (SSOA) is used to estimate optimal gains of the Conventional Proportional Integral and Derivative (PID) and fuzzy tuned based PID controllers. The dynamic system performance is considered by contrasting the outcomes with SSOA-optimized classical PID controllers and Fuzzy tuned PID controllers. The suggested SSOA with the Fuzzy tuned based PID controllers can maintain frequency within the acceptance range of the hybrid generating system under various perturbations and system instabilities, according to MATLAB/SIMULINK simulation study. Plotted and evaluated are the system's transient responses to the load disturbance that fluctuates stepwise and randomly caused by fuel cell, solar, and wind perturbation. This research demonstrates that the proposed fuzzy tuned-PID (FT-PID) controller outperforms this application's competition.

Keywords - Load Frequency Control (LFC), PID controller, Fuzzy Tuned PID controller (FT-PID), Salp Swarm Optimization Algorithm (SSOA).

1. Introduction

Frequency instability is a significant problem in large-scale electrical networks and a critical issue for power supply operators. The growing size of interconnected power systems has coincided with the emergence of oscillations frequency issues, which can lead to disconnection actions, line loss, and zone isolation. Wind speed varies throughout the year in a given location, causing changes in wind generators' output frequency and power. Photovoltaic production is also dynamic, as it is influenced by the surrounding environment [1]. Without applying sophisticated control strategies, regulating the frequency of hybrid power generation is challenging due to the erratic landscape of non-conventional energy resources. The result of non-conventional energy sources may have an impact on grid power. LFC is one of modern energy production's most significant load control ancillary services. The primary motive of LFC is to keep the balance between production and loads required as close to zero as possible, reducing frequency deviations.

While ensuring a high level of system reliability and keeping voltage and frequency within acceptable ranges, a power system that is well-designed and controlled should be able to handle adjustable loads and system disruptions [2]. Under varying loads required and erratic input power of wind, the wind side pitch controllers may not be capable of managing the system's frequency any further for wind power generation due to their poor reaction [3]. As a result, it is investigated how output frequency is affected by variations in load demand and renewable energy inputs.

Consequently, the importance of LFC in the strategy and process of electric power systems has been recognized. In a microgrid, the LFC regulates the actual power output of the generators to maintain the tie-flow line within predetermined tolerances and consider changing load requirements to keep each area's frequency within acceptable limits. To keep the load frequency constant, various methods and controllers have been used [4]. In the case of a system that integrates renewable energy sources, a manageable load is employed to

soak additional production to facilitate LFC [8]. The contribution of the paper is:

- The Fuzzy based proportionally–integral–derivative (PID) controller is utilized in Load Frequency Control (LFC), and Salp-Swarm Optimization Algorithm (SSOA) is used to tune PID controller gain constraints.
- A proposed MATLAB/SIMULINK modelling for a fuel cell, wind and solar-based hybrid system demonstrates that fuzzy-tuned PID controllers can proficiently sustain assessed frequency under the variation of load demand and fluctuating production from PV/wind sources.
- The best features of classical and fuzzy controllers have been combined, with equal weight given to each controller style.

The paper is organized as follows, the system's related work is described in Section 2, and the design elements of the proposed technique are highlighted in Section 3. In Sections 4 and 5, respectively, the mathematical modelling of the isolated hybrid power system and the optimization techniques used are covered. In Section 6, the simulation results are shown, examined, and debated. The planned work's conclusions are challenged in Section 7, which also covers the scope of subsequent work.

2. Related Work

In an integrated hybrid power system, load frequency control is crucial to managing load and generation frequency variation. Since RES electricity generation is unpredictable, it cannot be adequately predicted. In Ramli et al., it is possible to connect RESs to conventional power generation systems to create a dependable isolated hybrid power system (HPS) to get around RESs' unpredictable behaviour (IHPS). The cost and dependability of hybrid power systems are calculated using the metaheuristic optimization method with multiple goals and self-adaption, where the scope of hybrid microgrid system elements are also adjusted.

Two well-known metaheuristic approaches, optimization technique and harmony search (HS) in Guangqian et al., were used to determine the appropriate size of the HPS. A standalone hybrid power system (HPS) comprising a fuel cell, an aqua electrolyzer, a diesel-powered alternator, and a power generation system with wind power has been utilized [4]. To ensure a high-quality power supply, the impact of the developed system on load stabilization has been taken into account in this work. [5] describes the creation of a hybrid fuel cell and photovoltaic power system for standalone applications. This system's function is to produce electric energy at remote locations continuously. A hybrid battery, solar, and fuel cell system supplying an electric car have been modelled, controlled, and power managed [6].

The HPS model's scale, which contains fuel cell, solar, and wind, has been optimised using the artificial bee swarm optimization algorithm. The simulated work of [19] demonstrated the financial effectiveness of the developed HPS system. For modelling studies, [20] has taken into account the hybrid generation systems composed of fuel cells, PV, battery energy storage systems, WTGs, solar thermal power generation (STPG), DEGs, flywheels, super-capacitors, and aqua electrolyzers.[21-36]

3. Proposed Hybrid Microgrid Model Frequency Stabilization Based Salp-Swarm Optimization Algorithm (SSOA)

The model's upper portion, the turbine-governor part, is essentially identical to the traditional model aside from the representation of the turbine mechanical power variation (ΔP_M) caused by the governor's primary frequency control of the slow component (PM_0). The rapid element of the MW reaction is called ΔP_M.
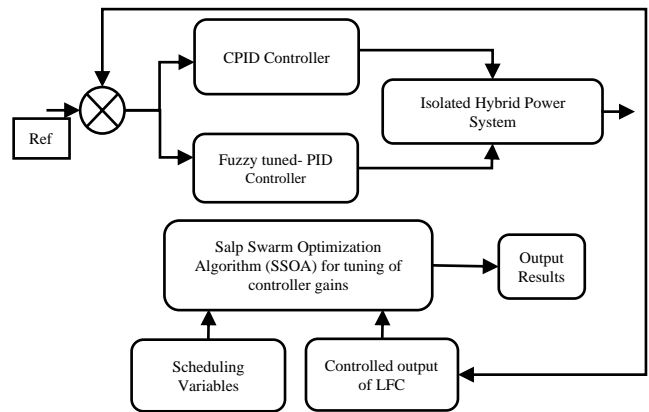

Fig. 1 Proposed block diagram-based Salp-Swarm Optimization Algorithm (SSOA)

The proposed Salp Swarm Optimization Algorithm (SSOA) block diagram, which uses solar, wind, and fuel cells as its primary energy sources, is shown in Figure 1. Using a photovoltaic system, solar energy is immediately turned into electricity [2]. Wind power is converted into mechanical power using a wind turbine alternator, where mechanical power production fluctuates dependent on the current speed of the wind. The wind turbine converts the mechanical energy it produces into electrical energy. Hydrogen was produced using a 10-kW electrolyzer and used as fuel in a 10kW Fuel Cell (FC) device to generate electricity.

The hybrid power system's electrical energy is delivered into the load frequency control, where the Salp-Swarm Optimization Algorithm is used to maintain frequency stability (SSOA). Power system frequency and load demand are inversely correlated. System stability requires a

frequency variation of zero. A component of the IHPS is connected to the frequency controller's output, designated as ΔP_c. It is impossible to directly control the frequencies of WTG, SPV, and SPS. Therefore, the frequency controller needs to be set up to control the IMG's overall frequency so that, in the event of an IMG disturbance, a balance between all the generating sources can be established.

4. Proposed Hybrid Power Systems Modeling
4.1. Modelling of Fuel Cell
The chemical energy of hydrogen or any other fuel is transformed directly into electrical energy by FCs, which are static energy conversion devices. Figure 2 displays a fuel cell transfer function model. The first-order TF of FC is expressed as a simplified form while ignoring non-linearities.

$$G_{FC}(S) = \frac{K_{FC}}{1+ST_{FC}} \tag{1}$$

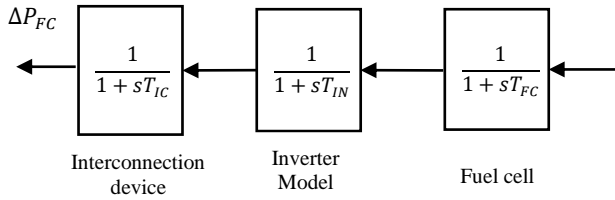Where, K_{FC} and T_{FC} are the gain and the time constant, respectively.

Fig. 2 Transfer function model of fuel cell

A part of the system's excess energy is sent to the electrolyzer, which converts it to hydrogen. The electrolyzer's transfer function is described as,

$$\Delta P_E = \frac{1}{1+sT_E}.\Delta F \tag{2}$$

4.2. Wind System Modelling
The Wind model's transfer function is of exceedingly high order and comprises many non-linearities. A second-order transfer function, on the other hand, can be used to represent the wind model. The electric generator and the wind turbine are the two primary components of the wind turbine model [10].
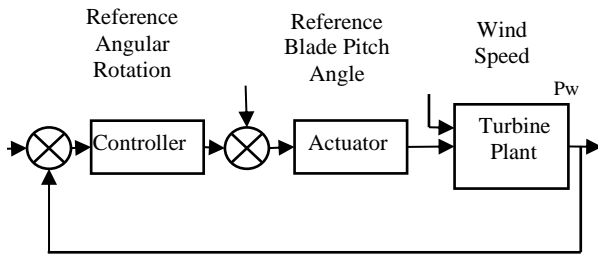

Fig. 3 Wind system model

The output power P_m Stays constant while the angular speed and aerodynamic torque are changed. A first-order system combines the electric generator and the wind turbine.

Figure 3 represents the wind system model, which illustrates that the wind model's control goal is to keep the rotational power and speed output constant. The rotational speed is fed back to accommodate changes in wind speed. The aerodynamic torque is controlled when the angle is handled and mechanical power is extracted. The wind turbine Transfer function is

$$G_{WT} = \frac{K_{WT}}{1+ST_{WT}} \tag{3}$$

The wind Generator Transfer function is

$$G_{WG} = \frac{K_{WG}}{1+ST_{WG}} \tag{4}$$

The gain constants of the wind turbine and wind generator models are KWT and KWG, respectively. TWT and TWG are the time constants of wind turbine and wind generator models. The WTG system converts the kinetic energy of moving air into electrical energy. The aerodynamic power turbine's (Pt) output power can be expressed as

$$p_t = \frac{1}{2}C_p(\lambda, \beta)\rho\pi R^2 v^3 \tag{5}$$

Where, ρ is the purpose of the pitch angle of the blade and the speed ratio of the tip; blade radius is denoted by R, the pitch angle is denoted by β, The linear wind speed is v, and the co-efficient of power is denoted by C_p. The transfer function expressions are shown in (6) – (10). The coupling block of fluid transmits speed at a rate that is inversely proportional to the modification between the frequencies of the generator and the turbine. The difference in power created in response to this is detailed in (6)

$$\Delta P_{GW} = K_{IG}(\Delta F_T - \Delta f) \tag{6}$$

Where, the WTG's speed deviation is referred as F_T. and K_{IG} is the fluid coupling gain. The wind turbine induction alternator's speed is represented in (7).

$$\Delta F_T = \left(\frac{1}{1+sT_W}\right)[K_{TP}\Delta F_T - \Delta P_{GW} + K_{PC}\Delta X_3 + \Delta P_{IW}] \tag{7}$$

Where, ΔX_3 is the data fit frequency response as a result, P_{IW} is the input power variation of wind (in p.u), and K_{PC} is the gain of blade characteristics. Simple lag compensation is provided via a data-fit frequency response block corresponding with the model's gain attributes. Data fit frequency response output can be displayed in (8).

$$\Delta X_3 = \Delta X_2 \left[\frac{K_{P3}}{1+sT_{P3}}\right] \qquad (8)$$

In (9), ΔX_2 is the hydraulic pitch actuator's output, K_{P3} is the statistics fit the frequency response block's gain, and T_{P3} is the block's constant time. The hydraulic pitch controller regulates the turbine's angle of pitch. The hydraulic pitch actuator's output can be stated by (9)

$$\Delta X_2 = \Delta X_1 \left[\frac{K_{P2}}{1+sT_{P2}}\right] \qquad (9)$$

In (9), ΔX_1 denotes the output of the pitch controller, K_{P2} denotes the hydraulic pitch controller's gain, and TP2 is the constant time (in seconds). The frequency angle must be carefully chosen to attain the WTG's maximum power output. The output of the frequency angle block can be derived by (10)

$$\Delta X_1 = \Delta P_{CW} \left(\frac{K_{P1}(1+sT_{P1})}{1+s}\right) \qquad (10)$$

Where, P_{CW} is the control signal for the pitch control block (in p.u.), K_{P1} is the gain for the pitch control block, and T_{P1} is the time constant for the pitch control block (in a sec).

4.3. Solar Panel Modelling

PV panel filters and Maximum Power Point Tracking (MPPT) inverters are all models for solar panels in the PV model. The solar cell output current and photocurrent equations determine the PV panel's transfer function. The MPPT is a method of getting the most power out of a solar panel. Examining the data yields the MPPT model boost converter's ON and OFF states. The PV model's transfer function is generated by combining all the components' transfer functions.

A solar cell is a key component of a PV module because it can convert photon energy into pollution-free electricity when coupled in series and parallel. These components are attached in parallel and series configurations to construct PV arrays, producing clean, green electricity. You can imagine a solar cell as a module of an electrical network. The Joule effect and interaction losses comprise a p-n junction diode, a photocurrent generator, and two resistors, one interconnected and the other in parallel. As a result, this configuration is recognized as a model of a single-diode solar cell model. The solar panel generator transfer function, is given by,

$$G_{SG} = \frac{K_{SG}}{1+ST_{SG}} \qquad (11)$$

In order to determine the output current,

$$I_C = I_{ph} - I_0 \left(e^{\frac{e}{AKT_C}(V_C+R_SI_C)} - 1\right) \cdot \frac{V_C+R_SI_C}{R_{Sh}} \qquad (12)$$

Where, E is described as elementary charge (1,10610-19 C); k = Boltzmann constant (0,13810-23 J/C); A = diode idealisation factor coefficient; I_{ph}= photo-induced current; I_0= reverse saturation current; I_C= operating current; V_C= operating voltage; T_C stands for ambient temperature in Kelvin; R_S stands for photovoltaic cell series resistance, which is influenced by the depth of the junction and the contact resistance [7]; R_{sh} stands for ground leakage current resistance. Because the series resistance of solar cells (R_S) is substantially more significant than the ground leakage current resistance (R_{sh}) the last half of (12) becomes irrelevant, and the formula (12) is simplified (13):

$$I_C = I_{ph} - I_0 \left(e^{\frac{e}{AKT_C}(V_C+R_SI_C)} - 1\right) \qquad (13)$$

The operational current of a photovoltaic cell (I_C), is a function of the output voltage (V_C), and the latter is influenced mainly by the load current, solar insulation level, and ambient temperature (14)

$$V_C = \frac{AKT_C}{e} \ln\left(\frac{I_{ph}+I_0-I_C}{I_C}\right) - R_SI_C \qquad (14)$$

Constants C_{SV} and C_{SI} can be used to explain changes in solar insulation levels [15]

$$C_{SV} = 1 + \beta_T\alpha_S(S_x - S_c) \qquad (15)$$

$$C_{SI} = 1 + \frac{1}{S_C}(S_x - S_C) \qquad (16)$$

Where, S_C is the solar insulation level measured at T_P=25°C and S_X is the solar insulation level for the predicted time of day. According to (17), the change in temperature ΔT_C brought on by the change in solar insulation level is as follows

$$\Delta T_C = \alpha_S(S_x - S_C) \qquad (17)$$

$$V_{CX} = C_{TV}C_{SV}V_C \qquad (18)$$

The temperature and solar radiation fluctuate in the solar PV cell. In this study, an arbitrarily variable solar power production system has been integrated by the IHPS model to deliver the actual-time results.

4.4. Mathematical Model of Hybrid Microgrid Power System for LFC

One of the most used commercial controllers is the PID Controller. Different design methodologies can be used for a mathematical plant model, and the controllers' parameters that fulfil the closed loop's transient and steady-state specifications can be established. The practice of fine-tuning controller parameters to obtain the optimum control response possible is known as controller tuning [11]. The PID

controller is adjusted in this paper utilizing the math-work technique for tuning PID controllers, which achieves the closed-loop stability, acceptable performance, and robustness goals of PID tuning. The gain of the PID has been fine-tuned to achieve a suitable combination of performance and robustness. By default, the math-work program selects a crossover frequency depending on plant dynamics. Then it creates a 60 °-point goal phase margin.

PID gains are computed whether changes are made to the bandwidth, phase margin, reaction time, or transient response. The controller's integral gain, overshoot, rise time, peak, settling time, gain and phase margin are determined. The constancy of the closed loop is also assessed. The first step in PID tuning is to choose P, which generates a highly oscillatory stable response when combined with D and I set to zero. Then, because P was chosen previously, the value D was chosen to accommodate for transitory performance. The I value is determined using the P and D values chosen in the preceding steps to ensure steady-state performance. Then, a wholly tuned PID controller is produced using P, I, and D values.

$$P + I\frac{1}{s} + D\frac{N}{1+N\frac{1}{s}} = 0 \tag{19}$$

Where, P is represented as proportional, D is represented as Derivative, I is represented as integral, and N is the filter coefficient.

Table 1. Solar PV parameter for LFC

S.No	Parameter	Value
1	Operating Voltage	38V
2	Operating Current	5.87A
3	No Load Voltage	44V
4	Nominal Power	210W
5	Surface area	$1.26m^2$
6	Efficiency Co-efficient	17.34%
7	Reference temperature	25°C
8	Solar irradiance	1000 at STC
9	Maximum Power Voltage	37.38V
10	Maximum power Current	8.56A

Table 1 shows the solar PV parameters for load frequency stabilization. A PV generator's input data might be the hourly solar radiation on a horizontal surface. Calculating the solar irradiation of PV.

$$P_{pv_{out}} = \frac{G}{G_{ref}}[1 + K_T(T_C - T_{ref})]P_{N-PV} \tag{20}$$

$$P_{N-PV} = P_{r_{pv}} * \eta_{pv} \tag{21}$$

$$T_c = T_{amp} + (0.026 \times G) \tag{22}$$

Where, G and G_{ref} are solar radiation (W/m2) and irradiation at reference conditions ($G_{ref} = 1000W/m^2$) respectively K_T is the temperature-dependent Maximum Power Factor ($K_T = -3.7 \times 10^{-3}$ (1/°C) for mono and polycrystalline silicon, T_{ref} is the PV cell temperature under ideal circumstances, T_c is cell temperature and T_{ref} is the ambient temperature.

Table 2. Parameters of the wind for LFC

S.No	Parameter	Value
1	Minimum rotor speed	9rpm
2	Rated speed of the rotor	18rpm
3	Diameter of rotor	60 m
4	Area of rotor	2827m2
5	Rated speed of the wind	14m/s
6	Inertia Constant	0.72s
7	Rated Speed	18 rpm
8	Rated Power	1.5 MW
9	Turbine Damping	14×10^6 Nms/rad
10	Rotor Inertia	6.1×10^6 kg/mm
11	Shaft Stiffness	83×10^6 Nm/rad

Table 2 lists the specifications needed for LPF. Wind speed calculates how much energy is available in the wind for each hour [23]. When calculating WT's output power, the wind speed at hub height is considered.

$$\frac{v}{v_{ref}} = \left(\frac{h_{hub}}{h_{ref}}\right)^\alpha \tag{23}$$

$$P_{wind_{turbine}} =$$

$$\begin{cases} 0 \\ v^3\left(\frac{P_{rated}}{v_{rated}^3 - v_{cut-in}^3}\right) - P_r\left(\frac{v_{cut-in}^3}{v_{rated}^3 - v_{cut-in}^3}\right) \\ P_{rated} \end{cases} \tag{24}$$

$$v_{cut-out} < v < v_{cut-in}$$

$$v_{cut-in} \leq v \leq v_{rated}$$

$$v_{rated} \leq v \leq v_{cut-out}$$

$$P_{wind} = P_{wind-turbine} * \eta_w \tag{25}$$

Where, v is the wind speed at the desired altitude ($h_{hub} = 40m$) in current time step and v_{ref} is the wind speed (m/s) at the height of the reference ($h_{ref} = 43.6m$). ($\alpha = 1/7$) and ($\alpha = 1.5$)is the coefficient of ground surface friction in a highly forested environment. P_{rated} is the rated wind turbine power $P_{rated} = 5KW$). v_{cut-in} is cut-in wind speed ($v_{cut-in} = 2.5m/s$), $v_{rated}$is rated wind speed ($v_{rated} = 9.5m/s$), $v_{cut-out}$is cut-out wind speed $v_{cut-out} = 40m/s$). The wind turbines may function effectively even in very little wind. The wind turbine's blade diameter is 6.4 metres. The product of pi and the square of the blade's radius determines the swept area, and the wind turbine's efficiency is 95%. The fuel cell's operational parameters are shown in Table 3.

Table 3. Operating point data of fuel cells for LFC

S.No	Parameters	Range
1	Load power rating	100kW
2	Rated load Voltage	254.42kW
3	Rated load Current	393.0696
4	Quantity of cells	384
5	Quantity of stacks	1 for 100Kw / 10 for 1MW
6	Cell Utilization	0.869
7	Voltage at the open circuit for every cell	0.935
8	Fuel supply volume	0.9e-3 kmol/s
9	Incoming airflow	1.8e-3 kmol/s
10	Tafel slope	0.11
11	Area of cell	$1000cm^2$
12	The average temperature of the cell	1000℃
13	Nominal Ohmic resistance	0.127

A fuel generator serves as a backup energy store during periods of peak demand. To determine the fuel generator's fuel usage,

$$F_{FG} = B_G \times P_{N-FG} + A_G \times P_{FG-out} \qquad (26)$$

Where, $P_{N-FG}(kW)$is the rated power. Every hour, there is an average load power requirement of 3.54 kW; hence, the rated power of the fuel generator is$P_{N-FG} = 4kW$ is considered.$P_{FG-out}$is the output power of the fuel generator.$A_G = 0.246l/kWh$ and$B_G = 0.08145l/kWh$ A_G

and B_G are fuel consumption coefficients (load/kWh).

5. Salp-Swarm Optimization Algorithm (SSOA)

In order to fine-tune the gains of proportional-integral-derivative (PID) controllers and fuzzy-tuned PID Regulators for (LFC) of a microgrid hybrid energy system, a novelty application of the salp swarm algorithm (SSOA) is developed in this paper. To imitate the foraging behaviour of the sea swarm slap, scientists have developed the Salp Swarm Optimization Algorithm (SSOA) [4]. The benefits of the SSOA as a novel heuristic optimization technique are reduced parameter needs and efficiency for continuous and discrete situations.

One species of Salpidae is the Salp, which has a transparent, jellyfish-like body with a length of 1 to 10 cm and a barrel-shaped form. Salps move by pumping water through their bodies as a kind of propulsion. They do not engage in active locomotion. Salp live in groups because they cannot effectively forage independently and need more food. When salps hunt in packs, they line up several of their prey to form a chain assembly (salp chain). The chain's initial salp is called the leader, and the following are followers.

The leader guides the entire chain, and the followers move around while adhering to one another [4]. Whereas the followers go according to local exploration, the leader directs them toward the food source for a global search. In the SSA, each follower's site upgrade will only be influenced by the location of the preceding follower, and the leader's site upgrade will only be influenced by the position of the food supply. The SSA's hierarchical structure forces the followers to work closely together to maximize optimization effectiveness and minimize the risk of being caught in a local optimum.

Algorithm 1: Pseudocode for Salp Swarm Optimization Algorithm
Initialize the salp population xi (i = 1, 2, ..., n) considering ub and lb
while (The final requirement is not achieved.)
Estimate each exploration agent's performance (salp)
F=the best search agent
Upgrade c1
for each salp (xi)
if (i==1)
Modify the leading salp's position.
Modify the follower Salp's location
end
end
Modify the salps based on the upper and lower boundaries of the variables.
end
return F

Table 4. Gain of the controllers

	Conventional PID converter					SSOA based Fuzzy tuned PID				
	K_P	K_I	K_D	Δf	Ts	K_P	K_I	K_D	Δf	Ts
Wind	0.13	0.0056	0.12	0.81	13.26	0.116	0.0036	0.10	-0.0089	4.15
Solar	0.105	0.0016	0.20	0.76	10.54	0.095	0.0012	0.13	-0.0076	3.98
Fuel cell	0.106	0.0018	0.32	0.67	11.43	0.085	0.0013	0.14	-0.0067	4.25
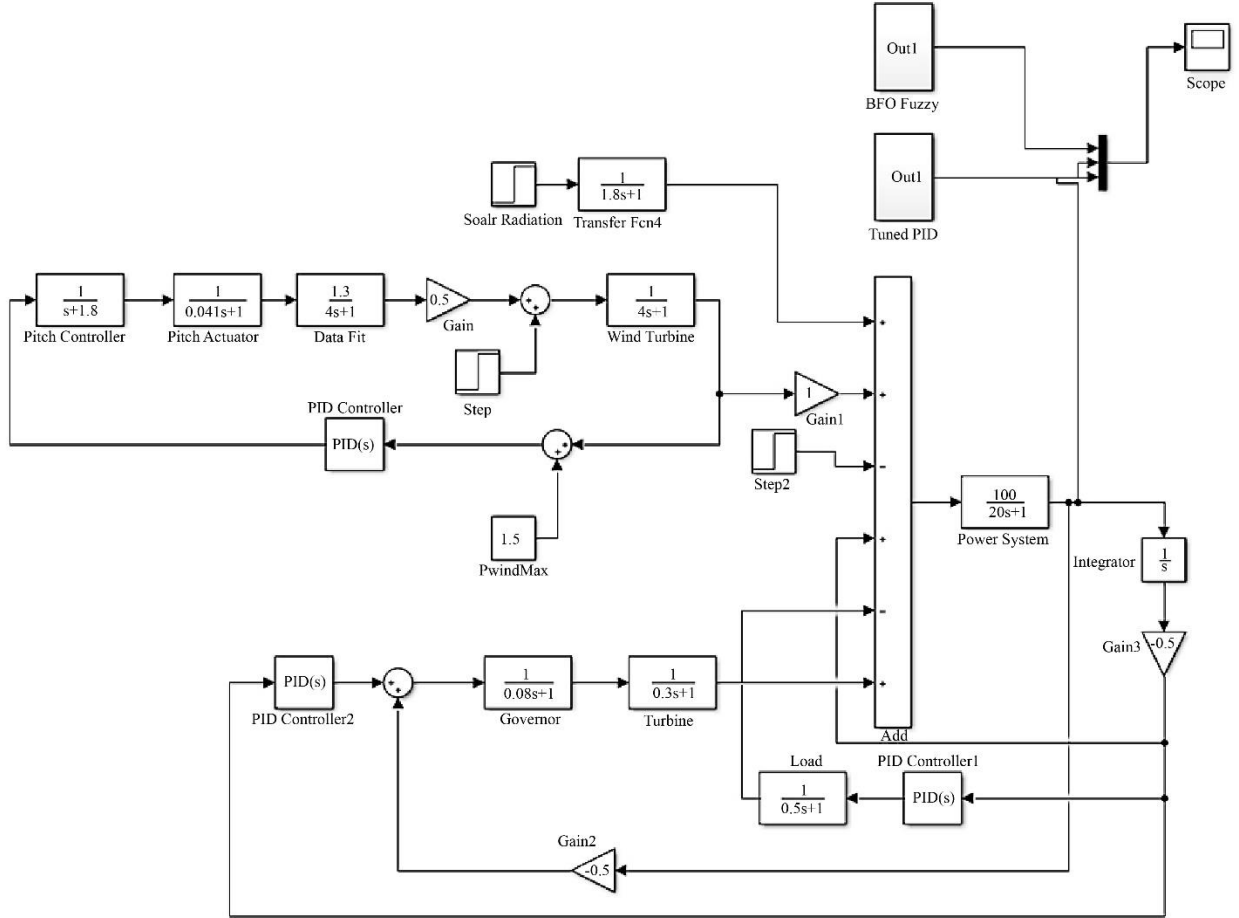
Fig. 4 Simulation diagram

The population is initially split into the leader and follower groups to model the salp chains mathematically. The salp at the forward-facing of the chain is the leader, while the other salps are referred to as followers. These salps have a leader who directs the swarm, and the followers obey the leader. In an n-dimensional exploration space, where n is the number of variables in a particular problem, the position of salps is specified. This is similar to other swarm-based algorithms. The positions of all salps are thus stored in a two-dimensional matrix named x. Additionally, the swarm is believed to use food source F as its target in the search space. The following equation is suggested as a means of updating the leader's position:

$$x_j^1 = \begin{cases} F_j + C_1\left(\left(Ub_j - lb_j\right)C_2 + lb_j\right) & C_3 \geq 0 \\ F_j - C_1\left(\left(Ub_j - lb_j\right)C_2 + lb_j\right) & C_3 < 0 \end{cases} \quad (27)$$

Where, x_j^1 represents the location of the leader in the jth dimension, F_j represents the food source is located in the Jth dimension, Ub_j and lb_j Stand for the upper and lower bounds of the jth dimension, correspondingly, and C_1, C_2 and C_3 stand for random integers. According to

equation (27), the leader merely alters its location in relation to the food supply. The most crucial factor in the SSOA is the coefficient c1, which balances exploitation and exploration as follows:

$$C_1 = 2e^{-\left(\frac{4l}{L}\right)^2} \tag{28}$$

L is the most repetitions possible, and l represents the current iteration. Random integers in the range [0,1] are generated uniformly for the parameters c2 and c3. In fact, they specify the step size and whether the next point in the jth dimension must be towards negative or positive infinity. Newton's law of motion is used in the following equations to upgrade the positions of the followers:

$$x_j^i = \frac{1}{2}at^2 + v_0t \tag{29}$$

x_j^1 displays the position of the ith follower salp in the jth dimension, t denotes time, v_0 denotes the beginning speed, and $a = v$ final v_0 where $v = x_t - x_0$. The inconsistency among iterations is equal to 1 because the time in optimization is iteration, and since v0 = 0, this equation can be written as follows:

$$x_j^i = \frac{1}{2}(x_j^i + x_j^{i-1}) \tag{30}$$

Where, $i \geq 2$ and x_j^i represents the location of the jth dimension's i^{th} follower salp with equations (27) and (30), the salp chains can be simulated.

6. Simulation Results and Discussion

The SSOA approach is used to optimise the controller gains. To analyze frequency dynamics under-load fluctuation, step loads are utilized. To determine frequency-varying aspects below abrupt changes in solar irradiation and speed of the wind, phase inputs for PV and wind are used. The simulation diagram for the proposed system is shown in Figure 4.

A ballistic load is also employed during mild loading to absorb extra energy generated by non-conventional resources. PID controller and the transfer function model are used to represent the system. The SSOA algorithm has been used to compute the best controller elements submitted to objective function minimization. Table 4 provides the controller gains at their optimum levels.

Figure 5 depicts the random variations in the IHPS model and lists the numerous inputs as load disturbance, fuel cell perturbation, wind and solar disturbance. The FEG and the WTG output fluctuate in reaction to sudden fluctuations in load trouble and wind perturbation, which also alters the considered model's frequency deviation response. The

adjustable parameters of the controllers are tuned using SSOA to eliminate the disturbance.
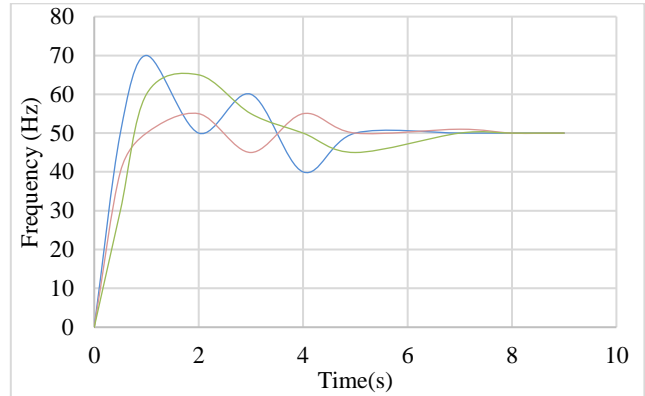
(a) During OFF peak load
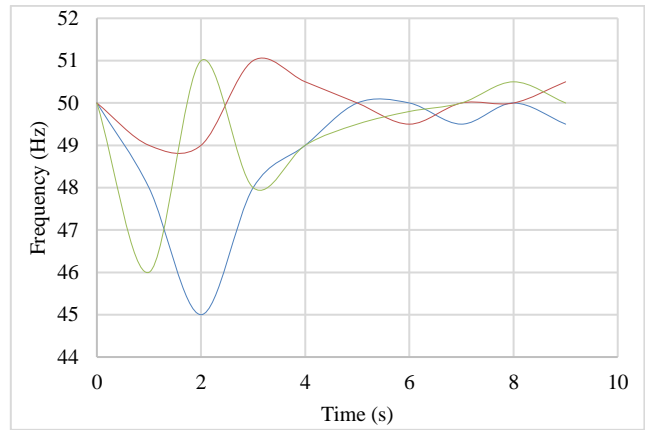
(b) During peak load
Fig. 5 Variation in frequency during off-peak and peak load

The relative frequency deviation profile of the controllers is completed after the gain parameter tweaking. Controllers (PID and fuzzy-tuned PID) are used to control this operation to adjust the discrepancy between the demand and production for the erratic shift in load demand.

Figure 6 shows the PID controller's simulation output for various load conditions. In this, the Kp, Ki and Kd value for the PID controller is 0.13, 0.0056 and 0.12, respectively, for wind, and 0.105, 0.0016 and 0.20, for thermal. Using the PID controller, the tuned response producing the peak overshoot is 30%, which takes time to attain a steady state.

Figure 7 shows the simulation output for various load conditions using the SSOA algorithm. In this, the kp, Ki, and Kd value for the SSOA algorithm is 0.116, 0.0036 and 0.10, respectively, for wind and 0.95, 0.0012 and 0.13 for thermal. Using the PID controller, the tuned response producing the peak overshoot is 10%, which takes little time to achieve a stable state. The proposed SSOA algorithm produced better results than the conventional PID controller.
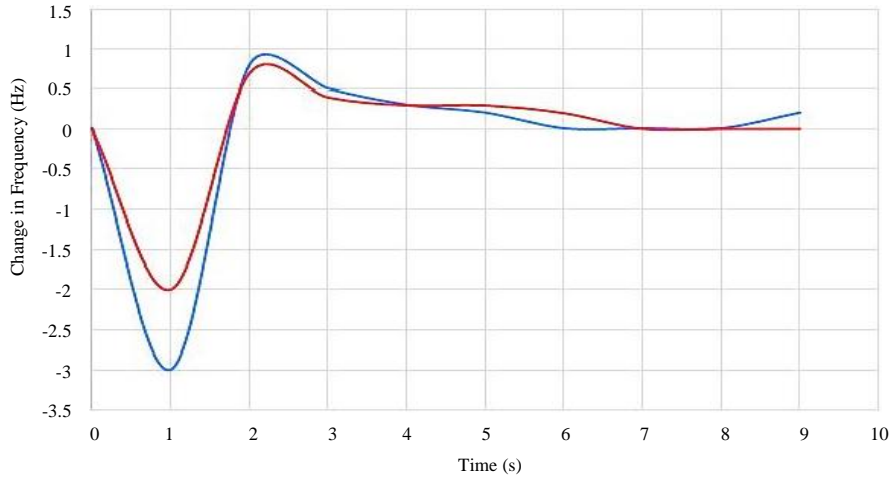
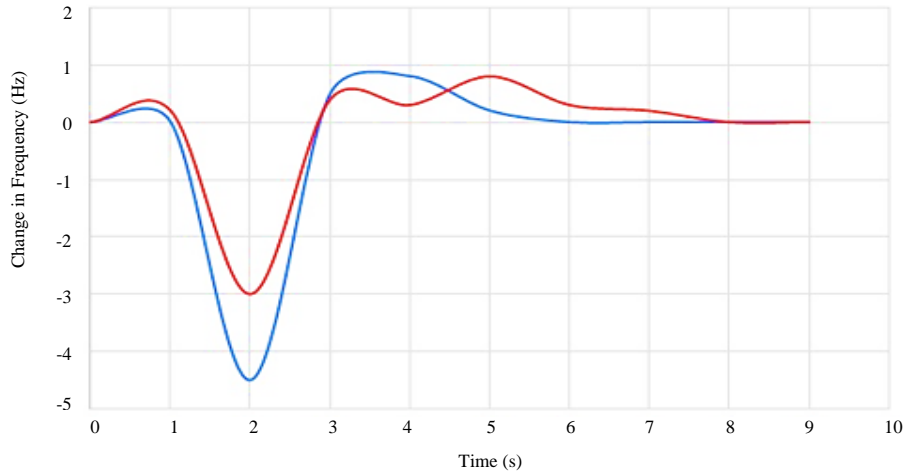**Fig. 6 Simulation output for various load conditions using PID controller**

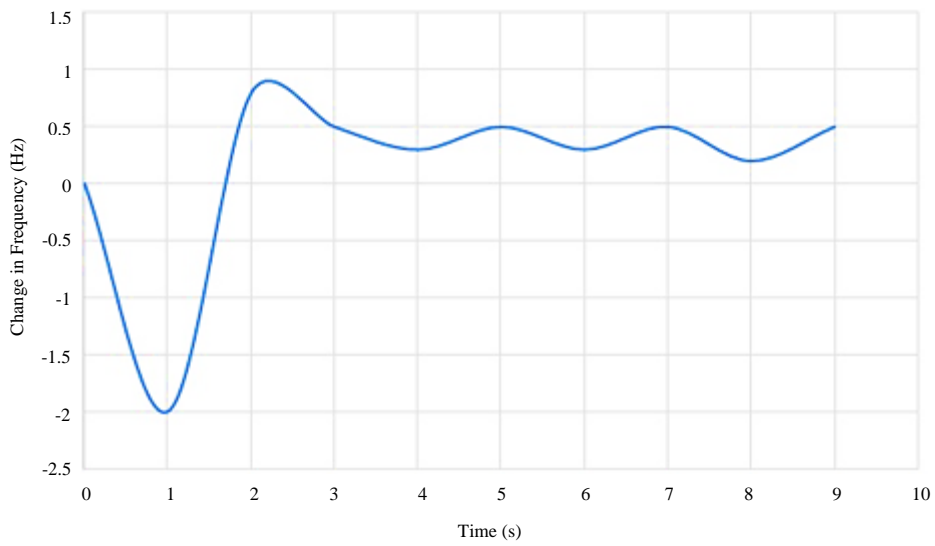**Fig. 7 Simulation output for various load conditions using the SSOA algorithm**

Fig. 8 Simulation output response of tuned PID controller with the response of the fuzzy-tuned controller
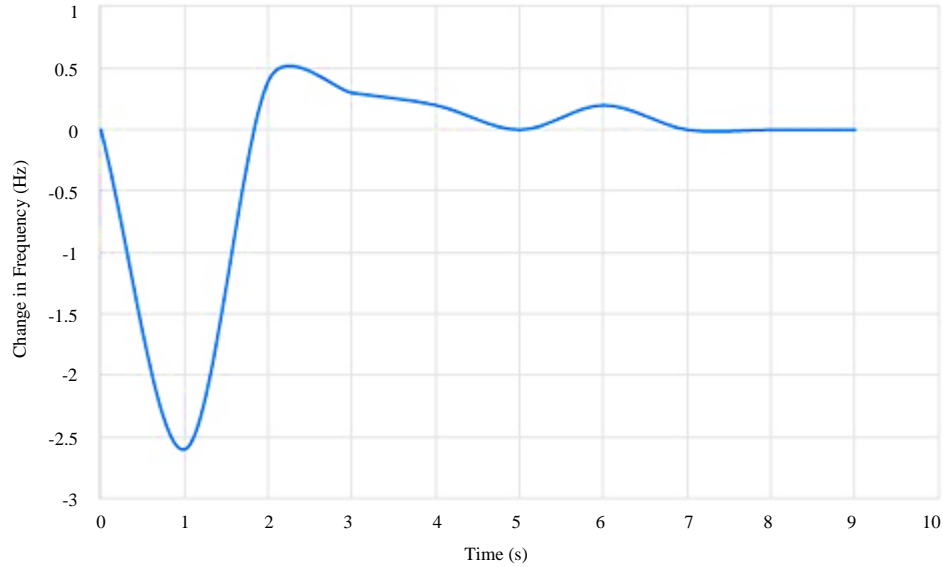
Fig. 9 Simulation output response of tuned SSOA-based fuzzy logic controller

Figure 8 shows the simulation output response of the tuned PID Controller. Using the PID controller, the tuned response produces the peak overshoot of 30% and its oscillations. It takes more time to achieve a steady state.

Figure 9 shows the simulation output response of a tuned SSOA-based Fuzzy logic controller. In this produced, the peak overshoot is only 8%. Compared to the conventional controller, the SSOA-based Fuzzy-solved settling time is better than the PID controller. That SSOA-based Fuzzy logic controller attains steady-state response very early compared to the PID controller. According to the simulation's findings, the SSOA-based Algorithm can regulate the system reliability and stability of the microgrid by making sure that the stability of frequency and voltage-controlled restrictions and deviation, as well as proper power-sharing, take place when the microgrid is in island mode, and a load is changed.

7. Conclusion
This paper aimed to simulate and analyze the performances of conventional PID controllers and fuzzy tuned based PID controllers in fuel cell-wind-PV-based power generation systems using Salp Swarm Optimization Algorithm (SSOA). In the proposed LFC, the gain parameters of the utilised controllers are determined using

the SSOA algorithm. Using a controller, a ballistic load absorbs extra power produced by non-conventional energy sources. Under step changes in load and the production of non-conventional energy, the performance of the planned LFC is examined.

The study unequivocally demonstrates that SSOA-tuned fuzzy-based PID controllers provide significantly superior LFC performance compared to traditional PID controllers. The comparative simulation and analysis of two alternative controllers show that the proposed SSOA-based fuzzy adjusted PID-controlled IHPS model performs better in both cases, delivering real objective function values and performance indices at a rate of 96% efficiency. Future additions of energy storage devices and the creation of a robust controller that can increase the stability and dependability of the system may be made to the researched IHPS model.

Appendix
Generating systems simulation system parameters are given below:

Frequency of F=50Hz, D=0.25, H=10s, T_{SG}=0.08s T_T=0.3s, Tps=2H/f D=1.5s, Tw=1.0s. K_{PV}=1.6s, K_W=1.0.

References
[1] M. W. Siti et al., "Application of Load Frequency Control Method to a Multi-Microgrid with Energy Storage System," *Journal of Energy Storage*, vol. 52, 2022. [CrossRef] [Google Scholar] [Publisher Link]

[2] Luis M. Castro, "Simulation Framework for Automatic Load Frequency Control Studies of VSC-Based AC/DC Power Grids," *International Journal of Electrical Power and Energy Systems*, vol. 141, 2022. [CrossRef] [Google Scholar] [Publisher Link]

[3] Abhishek Saxena, and Ravi Shankar, "Improved Load Frequency Control Considering Dynamic Demand Regulated Power System Integrating Renewable Sources and Hybrid Energy Storage System," *Sustainable Energy Technologies and Assessments*, vol. 52, 2022. [CrossRef] [Google Scholar] [Publisher Link]

[4] Jizhen Liu, Qi Yao, and Yang Hu, "Model Predictive Control for Load Frequency of Hybrid Power System with Wind Power and Thermal Power," *Energy*, vol. 172, pp. 555-565, 2019. [CrossRef] [Google Scholar] [Publisher Link]

[5] Xichao Zhou et al., "Actuator Fault-Tolerant Load Frequency Control for Interconnected Power Systems with Hybrid Energy Storage System," *Energy Reports*, vol. 6, no. 9, pp. 1312-1317, 2020. [CrossRef] [Google Scholar] [Publisher Link]

[6] Asma Aziz, Aman Than Oo, and Alex Stojcevski, "Analysis of Frequency Sensitive Wind Plant Penetration Effect on Load Frequency Control of Hybrid Power System," *International Journal of Electrical Power and Energy Systems*, vol. 99, pp. 603-617, 2018. [CrossRef] [Google Scholar] [Publisher Link]

[7] Pan S. Das, "Fractional Order Fuzzy Control of Hybrid Power System with Renewable Generation using Chaotic PSO," *ISA Transactions*, vol. 62, pp. 19-29, 2016. [CrossRef] [Google Scholar] [Publisher Link]

[8] Rabindra Kumar Sahu et al., "Teaching Learning Based Optimization Algorithm for Automatic Generation Control of Power System using 2- DOF PID Controller," *International Journal of Electrical Power and Energy Systems*, vol. 77, pp. 287-301, 2016. [CrossRef] [Google Scholar] [Publisher Link]

[9] S. Ganguly, T. Mahto, and V. Mukherjee, "Integrated Frequency and Power Control of an Isolated Hybrid Power System Considering Scaling Factor Based Fuzzy Controller," *Swarm and Evolutionary Computation*, vol. 32, pp. 184-201, 2017. [CrossRef] [Google Scholar] [Publisher Link]

[10] Saroj Kumar Mishra, and Subhranshu Sekhar Pati, "Load Frequency Control of Multi-source System by Jaya Optimized Fractional Order PID Controller," *2020 7th International Conference on Smart Structures and Systems (ICSSS)*, India, pp. 1-5, 2020. [CrossRef] [Google Scholar] [Publisher Link]

[11] Sandro Sitompul, and Goro Fujita, "Implementation of BESS Load Frequency Control in Islanded Microgrid System by Considering SOC," *In 2020 IEEE PES Innovative Smart Grid Technologies Europe (ISGT-Europe)*, pp. 980-984, 2020. [CrossRef] [Google Scholar] [Publisher Link]

[12] Chunyu Chen et al., "Tie-Line Bias Control Applicability to Load Frequency Control for Multi-Area Interconnected Power Systems of Complex Topology," *Energies*, vol. 10, no. 1, pp. 1-15, 2017. [CrossRef] [Google Scholar] [Publisher Link]

[13] Xiao Zhaoxia et al., "Flat Tie-Line Power Scheduling Control of Grid-Connected Hybrid Microgrids," *Applied Energy*, vol. 210, pp. 786-799, 2018. [CrossRef] [Google Scholar] [Publisher Link]

[14] Diambomba Hyacinthe Tungadio, and Yanxia Sun, "Load Frequency Controllers Considering Renewable Energy Integration in Power System," *Energy Reports*, vol. 5, pp. 436-453, 2019. [CrossRef] [Google Scholar] [Publisher Link]

[15] R. Ahshan et al., "Micro-Grid System Based on Renewable Power Generation Units," *Canadian Conference on Electrical and Computer Engineering*, Canada, pp. 1-4, 2010. [CrossRef] [Google Scholar] [Publisher Link]

[16] K. M. G. Y. Sewwandi et al., "Wind Turbine Emulator for a Microgrid," *2017 Innovations in Power and Advanced Computing Technologies (i-PACT)*, India, pp. 1-6, 2017. [CrossRef] [Google Scholar] [Publisher Link]

[17] Amandeep Singh, and Sathans Suhag, "Frequency Regulation in an AC Microgrid Interconnected with Thermal System Employing Multiverse-Optimised Fractional Order-PID Controller," *International Journal of Sustainable Energy*, vol. 39, no. 3, pp. 250-262, 2020. [CrossRef] [Google Scholar] [Publisher Link]

[18] F. Dubuisson et al., "Global Maximum Power Point Tracking Strategy Based on BFO Method for Standalone PV System under Partial Shading Conditions," *IECON 2021-47th Annual Conference of the IEEE Industrial Electronics Society*, Toronto, Canada, pp. 1-5, 2021. [CrossRef] [Google Scholar] [Publisher Link]

[19] F. Dubuisson et al., "A Bacterial Foraging Optimization Technique and Predictive Control Approach for Power Management in a Standalone Microgrid," *2020 IEEE Electric Power and Energy Conference (EPEC)*, Canada, pp. 1-7, 2020. [CrossRef] [Google Scholar] [Publisher Link]

[20] Kallol Roy et al., "Analysis of Energy Management in Micro Grid-A Hybrid BFOA and ANN Approach," *Renewable and Sustainable Energy Reviews*, vol. 82, no. 3, pp. 4296-4308, 2018. [CrossRef] [Google Scholar] [Publisher Link]

[21] V. Devaraj, and M. Kumaresan, "An Elite LOA-TFWO Approach for Load-Frequency Control of Islanded Micro-Grids Incorporating Renewable Sources," *International Journal of Engineering Trends and Technology*, vol. 70, no. 10, pp. 166-187, 2022. [CrossRef] [Publisher Link]

[22] Seyedali Mirjalili et al., "Salp Swarm Algorithm: A Bio-Inspired Optimizer for Engineering Design Problems," *Advances in Engineering Software*, vol. 114, pp. 163-191, 2017. [CrossRef] [Google Scholar] [Publisher Link]

[23] Farhad Zishan et al., "Allocation of Renewable Energy Resources in Distribution Systems while Considering the Uncertainty of Wind and Solar Resources via the Multi-Objective Salp Swarm Algorithm," *Energies*, vol. 16, no. 1, pp. 1-17, 2023. [CrossRef] [Google Scholar] [Publisher Link]

[24] Amitkumar Manekar, "Combined Dragonfly and Whale Optimization Algorithm for Cost and Energy Optimization in Resource Allocation and Migration," *International Journal of Recent Engineering Science*, vol. 10, no. 3, pp. 17-22, 2023. [CrossRef] [Publisher Link]

[25] Ibrahim Altawil et al., "Optimization of Fractional Order PI Controller to Regulate Grid Voltage Connected Photovoltaic System Based on Slap Swarm Algorithm," *International Journal of Power Electronics and Drive Systems (IJPEDS)*, vol. 14, no. 2, pp. 1184-1200, 2023. [CrossRef] [Google Scholar] [Publisher Link]

[26] Vinothkumar C, and Esakkiappan C, "Optimization of PI Controller on Level Control of Hopper Tank System with PSO Technique," *International Journal of Engineering Trends and Technology*, vol. 69, no. 10, pp. 178-185, 2021. [CrossRef] [Publisher Link]

[27] Debidasi Mohanty, and Sidhartha Panda, "Multi-Objective Salp Swarm Algorithm-Based Fractional Order Fuzzy Precompensated PDPI Controller for Frequency Regulation of Hybrid Power System," *International Journal of Numerical Modelling: Electronic Networks, Devices and Fields*, 2023. [CrossRef] [Google Scholar] [Publisher Link]

[28] R. Karthik Kumar, "Fuzzy Tuned PI Controller for Shunt Active Power Filter," *International Journal of Recent Engineering Science*, vol. 7, no. 6, pp. 23-30, 2020. [CrossRef] [Google Scholar] [Publisher Link]

[29] Zvikomborero Hweju, and Varaidzo Sostina Dandira, "Predicting the Capacitance of Parallel Plate Capacitors using Adaptive Neuro-Fuzzy Inference System (ANFIS)," *International Journal of Recent Engineering Science*, vol. 7, no. 5, pp. 26-28, 2020. [CrossRef] [Google Scholar] [Publisher Link]

[30] Mandeep Sharma, Surya Prakash, and Sahaj Saxena, "Robust Load Frequency Control using Fractional-Order TID-PD Approach via Salp Swarm Algorithm," *IETE Journal of Research*, pp. 1-17, 2021. [CrossRef] [Google Scholar] [Publisher Link]

[31] Prakash Chandra Sahu et al., "Improved-Salp Swarm Optimized Type-II Fuzzy Controller in Load Frequency Control of Multi Area Islanded AC Microgrid," *Sustainable Energy, Grids and Networks*, vol. 16, pp. 380-392, 2018. [CrossRef] [Google Scholar] [Publisher Link]

[32] G. Dinesh, "A Modified Self Tuning Fuzzy Logic Controller for Brushless Direct Current Motor," *International Journal of Recent Engineering Science (IJRES)*, vol. 1, no. 1, pp. 22-27, 2014. [Publisher Link]

[33] Idriss Dagal, Akın Burak, and Erdem Akboy, "MPPT Mechanism Based on Novel Hybrid Particle Swarm Optimization and Salp Swarm Optimization Algorithm for Battery Charging through Simulink," *Scientific Reports*, vol. 12, no. 1, pp. 1-17, 2022. [CrossRef] [Google Scholar] [Publisher Link]

[34] Ismail Akbar Khan et al., "Salp Swarm Optimization Algorithm-Based Fractional Order PID Controller for Dynamic Response and Stability Enhancement of an Automatic Voltage Regulator System," *Electronics*, vol. 8, no. 12, pp. 1-17, 2019. [CrossRef] [Google Scholar] [Publisher Link]

[35] Nitesh M Sureja, and Sanjay P. Patel, "An Improved Particle Swarm Optimization Algorithm for A Variant of TSP," *SSRG International Journal of Computer Science and Engineering*, vol. 7, no. 5, pp. 16-20, 2020. [CrossRef] [Publisher Link]

[36] Touqeer Ahmed Jumani et al., "Salp Swarm Optimization Algorithm-Based Controller for Dynamic Response and Power Quality Enhancement of an Islanded Microgrid," *Processes*, vol. 7, no. 11, pp. 1-19, 2019. [CrossRef] [Google Scholar] [Publisher Link]